Impact of the Initial Flow Conditions on the Wetting Efficiency on a Flat Inclined Surface

D. Asendrych

The paper presents a numerical study of a liquid flow on a flat inclined surface using a 3-dimensional unsteady Eulerian multiphase model. Application of a VOF (Volume of Fluid) technique, a surface tracking method, allowed to reconstruct a flow structure and determine surface wettability revealing their dependence on the liquid flow rate. The critical Reynolds number value corresponding to the transition from the rivulet flow to the fully wetted surface was found to agree quite well with the reference literature data. Detailed calculations showed that the solution is sensitive to the initial conditions, i.e. it may change when the dry plate is replaced by a surface covered with a liquid film. Such a behaviour results from variation of the dynamic contact angle between the receding and the advancing contact angles corresponding to the dewetting and wetting conditions, respectively.

1   Introduction

Packed bed columns are commonly used in various industrial installations in chemical, process, petrochemical and the other sectors. The efficiency of such processes like absorption (Niegodajew and Asendrych, 2016), drying, distillation, or rectification (Haroun et al., 2014) is strongly dependent on the ability of the column packing to enlarge the contact area between co- or counterflowing phases and in turn to enhance the mass, momentum and heat transfer processes. Among the factors influencing the effective area of the liquid free surface, one can mention the packed bed characteristics (porosity, specific surface area, liquid spreading ability), gas and liquid properties (Lappalainen et al., 2008) as well as their loads (Asendrych and Niegodajew, 2017). The complexity of the problem makes the optimisation of packed bed columns challenging. That is why a deeper understanding of the flow hydrodynamics for much simpler geometries as flat or textured surfaces is required.

In the existing literature a number of studies is devoted to the liquid flow structure on flat surfaces, just to mention the works of Haroun et al. (2012), Haroun et al. (2014), Xu et al. (2008) or Xu et al. (2012). The main finding of these works is the evolution of the liquid flow structure upon the flow rate or Reynolds number. With its increase flow evolves from droplet-like flow through the system of rivulets up to film flow completely covering the surface. The other papers approach more complex systems. For instance Xu et al. (2014) investigated gas-liquid-liquid system consisting of two immiscible liquids of significantly different surface tensions. Moreover, the influence of a counterflowing gas phase on liquid behaviour was taken into account. In order to capture that effect the drag force was included in the momentum equation with the drag force coefficient proposed by Stephan and Mayinger (1992). Another important aspect approached in the literature is the influence of liquid properties on the wetting efficiency. The surface tension and the contact angle turned out to be of special importance as they may cause significant change of the morphological flow structure and in turn the portion of wetted surface. These parameters were investigated parametrically by Singh et al. (2017) and Asendrych (2018) showing the relevance of the Weber and Kapitza numbers in quantifying these effects.

A step forward was to consider corrugated surface shape in the model (see e.g. Iso et al., 2013, Subramanian and Wozny, 2012, Szulczewska et al., 2003 and Haroun et al., 2012) imitating the geometry of industrially available structured packings. The geometrical constraints of the flow were usually limited to a single element of the packing of relatively small extents, thus ensuring reasonable computational times. Sebastia-Saez et al. (2015a) and Haroun et al. (2012) employed CFD to determine the liquid holdup and the gas pressure drop. Another direction of numerical works was to include physical (Haroun et al., 2012, Sebastia-Saez et al., 2013, Sebastia-Saez et al., 2014b and Xu et al., 2009) and reactive (see e.g.: Haroun et al., 2010, Sebastia-Saez et al., 2014a and Sebastia-Saez et al., 2015b) mass transfer processes taking place at gas-liquid interface. The most advanced model incorporating various aforementioned phenomena was proposed by Sebastia-Saez (2016) and it was employed to predict the carbon dioxide capture in the aqueous solution of amine solvent.

In the present paper a numerical model enabling the reconstruction of the flow structure on a flat surface was developed. The aim of the research was to test the model for simple geometry and make it ready to apply to more complex cases simulating industrial designs of structured packings for various flow conditions. Additionally the influence of initial conditions on the solution and wetting efficiency was studied.

2   Numerical Model

The liquid flow structure was simulated with the use of a 3-dimensional (3D) multiphase Eulerian model. The flow was considered as unsteady, isothermal and laminar, with water as the liquid phase and air as the surrounding medium being in rest. Both fluids were treated as Newtonian and incompressible and not interpenetrating. Therefore the Volume of Fluid (VOF) model was employed to track the interface (i.e. liquid free surface) between immiscible fluids. The mutual interactions between fluidic phases were neglected. The properties of fluids, i.e. density, viscosity and surface tension were assumed to be equal to those at ambient conditions. In particular the water surface tension σ and the static contact angle α of the water-stainless steel system were set to 72.8 mN/m and 70°, respectively.

2.1. Governing Equations

The VOF formulation is based on the assumption that the phases are not interpenetrating. For the ith phase an additional variable called volume fraction γ_i is introduced. It is defined as the ratio of the ith phase volume and the total volume:

$$\gamma_i = V_i / \sum_i^n V_i \tag{1}$$

where n is a number of phases. Obviously in each cell the volume fractions of all mixture components meet the following condition:

$$\sum_{i=1}^n \gamma_i = 1 \tag{2}$$

When VOF model is employed all flow variables and mixture properties (i.e. density ρ and viscosity μ) are shared by phases and represent volume-averaged values with local γ_i values used as weighting coefficients. Thus, for instance, the mixture density is given by:

$$\rho = \sum_{i=1}^n \gamma_i \rho_i \tag{3}$$

With the use of the VOF method the tracking of the interface between two phases is carried out by solving the continuity equation for the volume fraction of one of the phases (Ansys Inc., 2016). For the ith phase this equation takes the following form:

$$\frac{\partial (\gamma_i \rho_i)}{\partial t} + \nabla (\gamma_i \rho_i U_i) = 0 \tag{4}$$

Momentum equation is formulated for the mixture of phases. Except for the typical terms, it includes additionally the surface tension and the gravity forces:

$$\frac{\partial (\rho U)}{\partial t} + \nabla (\rho U \cdot U) = -\nabla p + \nabla \left[\mu \left(\nabla U + \nabla U^T \right) \right] + \rho g + S \tag{5}$$

Surface tension, being a result of forces attracting the fluid molecules, is implemented according to the model proposed by Brackbill et al. (1992). Continuum surface model (CSM), allowing to convert a surface force to a volumetric one, leads to the following expression for the source term S for the mixture composed of two fluids:

$$S = \sigma \frac{\rho \kappa \nabla \gamma_L}{(\rho_L + \rho_G)/2} \tag{6}$$

In order to define adequately the boundary condition at the inlet, an expression for the liquid film thickness δ was adopted from the work of Nusselt (1916):

$$\delta = \left[\mathrm{Re}_L \frac{3(\mu_L / \rho_L)^2}{g \sin \varphi} \right]^{1/3} \qquad (7)$$

where φ is the plate's inclination angle and Re_L is the liquid Reynolds number given by the following definition

$$\mathrm{Re}_L = \frac{\rho_L U_{mean} \delta}{\mu_L} \qquad (8)$$

based on the liquid film thickness and its mean velocity U_{mean}.

2.2. Computational Domain and Boundary Conditions

Computational domain was defined as a cuboid (see Figure 1) of the following dimensions: 60mm (length), 50mm (width) and 10mm (height). The length and width were chosen to fit the dimensions of the experimentally studied cases (Haroun et al., 2014 and Hoffmann et al., 2006), while the height had to ensure no impact of the top boundary on the liquid behaviour. Inclination angle was set to φ=60° for consistency with literature. The coordinating system was adjusted to the plate inclination (as shown in Figure 1) with its origin attached to the centre of the inlet plate's edge. Thus the abscissa is parallel to the surface and the ordinate perpendicular to it.
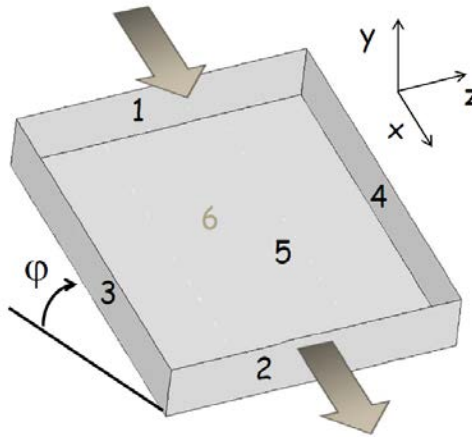

Figure 1. The view of the computational domain showing the plate's inclination angle φ and the flow boundaries with numbers corresponding to the boundary conditions (see Table 1): inlet (1), outlet (2), side walls (3) and (4), top boundary (5) and plate (6)

No	Boundary Condition	Settings
1	Velocity Inlet	i) near-wall zone, i.e. $0 < y \leq \delta$ - liquid volume fraction = 1 - parabolic velocity profile ii) outer zone, i.e. $y > \delta$ - liquid volume fraction = 0 - velocity = 0
2	Pressure Outlet	overpressure $p = 0$
3,4,5	Wall	non-slip condition, specified shear stress = 0, static contact angle = 70°
6	Wall	slip condition, static contact angle = 70°

Table 1. Boundary conditions set at the boundaries of the computational domain

In order to simulate the flow behaviour in a realistic way a system of boundary conditions was set at the domain boundaries which are summarized in Table 1. The velocity inlet boundary condition (liquid volume fraction distribution and parabolic velocity profile within the liquid film) was set with the use of a User Defined Function (UDF), a set of subroutines written in C language and linked to the solver. The UDF could be additionally utilised to initialize the solution with a liquid film covering the entire plate. Its thickness and velocity distribution were then set identically as at the inlet to the domain to avoid flow disturbance and speed up the convergence.

2.3. Numerical Tools and Settings

Ansys Workbench v.17 commercial simulation package was employed to solve the problem. Ansys DesignModeller was used to create a geometry, Ansys Mesher for discretization of computational domain and Ansys Fluent to solve the fluid flow. The VOF multiphase model was used with explicitly formulated volume fraction. The air was treated as a primary phase and water as a secondary one. Spatial discretization was performed with second-order upwind scheme for momentum, while the PRESTO! algorithm was used for pressure. Relaxation factors were kept at default levels, i.e. 0.7 for momentum, 0.3 for pressure, and 1.0 for density and body forces. Pressure-velocity coupling was done with the use of the PISO method. For the reconstruction of air-water interface the "geo-reconstruct" scheme was employed. For the time advancement a first order implicit scheme was utilised.

3 Simulation Results

Before the model was used for the simulations of surface wettability it had been tested in terms of spatio-temporal discretization. In order to better control the space discretization the computational domain was divided into 2 zones separated by the plane parallel to the plate. The position of the demarcation surface (4mm above the plate) was chosen in a way to ensure that the gas-liquid interface is completely included in a wall-adjacent region. Various meshing strategies were applied to ensure sufficient spatial resolution in that sensitive zone. Several meshes were tested with a total number of cells varying between 320 thousand and 1.46 million. Finally the mesh comprising 1.13 million cells was chosen as ensuring the grid-independent solutions for entire range of Reynolds numbers foreseen for analysis. Figure 2 presents the view of the final mesh, with the cell size progressively refined towards the surface, allowing to resolve the flow where the highest gradients of flow quantities (velocity, volume fraction) were expected. Above the demarcation surface the uniform coarse mesh was applied - see top part in Figure 2.
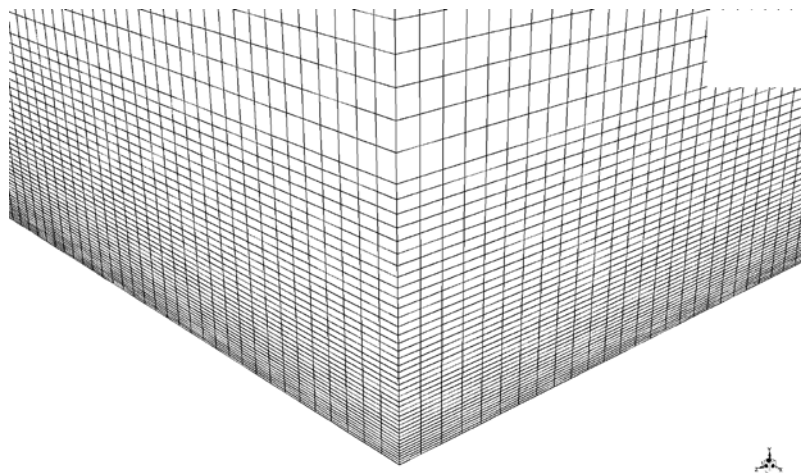

Figure 2. Magnified view of the numerical grid in the wall-adjacent corner of the domain

The time step tests were conducted in the range $10\mu s$ - $300\mu s$. A step of $25\mu s$ was found to ensure the best compromise between accuracy and computational times for all the Reynolds numbers planned for simulations.

3.1. Flow structure versus Reynolds Number

In order to identify the morphological structure of liquid flow in detail a series of simulations were performed for varying Reynolds number, constant inclination angle $\varphi = 60°$ and water with its material properties corresponding to the ambient conditions.

The 3-dimensional views of the gas-liquid interfaces for $Re = 50, 90, 130$ are presented in Figure 3. For all the cases the solution was initialized with "wetted" plate, i.e. the domain was filled in with a water film of relevant thickness and velocity profile. The interfaces are shadowed to provide the information about their elevations over the plate's surface. Black colour corresponds to the plate's level, while white one to the highest altitude. The same scale is applied to all three images shown in Figure 3.
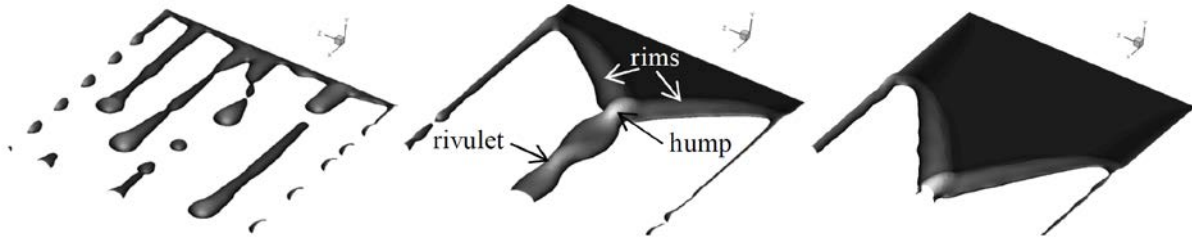

Figure 3. Flow structure evolution with Reynolds number: $Re = 50$ - droplet-like flow (left), $Re = 90$ - rivulet flow (centre), $Re = 130$ almost film flow (right)

The flow structure for $Re = 50$ (see Figure 3, left) is characterised by the presence of small rivulets breaking up into droplets. The liquid film is practically invisible. Such a flow behaviour indicates domination of the surface tension forces over the liquid inertia resulting in low wettability of the surface. When the Reynolds number increases to $Re = 90$ inertial effects become stronger, thus a portion of plate's surface is covered by the liquid film (see Figure 3, centre) with perfect wettability. At certain distance downstream the inlet edge the capillary pressure leads to formation of a stationary front resulting in liquid accumulation in elevated rims. Then liquid is redirected towards the plate's centre where two streams meet together creating a hump (with a whitish top). As a consequence local velocity rises giving finally birth to a rivulet. Further increase in the Reynolds number moves downstream the rivulet formation. Consequently portion of the plate covered with the liquid film enlarges and improves surface wettability. For $Re = 130$ (see Figure 3, right) inertial forces are strong enough to move the hump to the outlet edge further increasing the wetted surface. The presented morphological flow structure evolution with the Reynolds number is fully consistent with the observations of Xu et al. (2014) and Haroun et al. (2014).
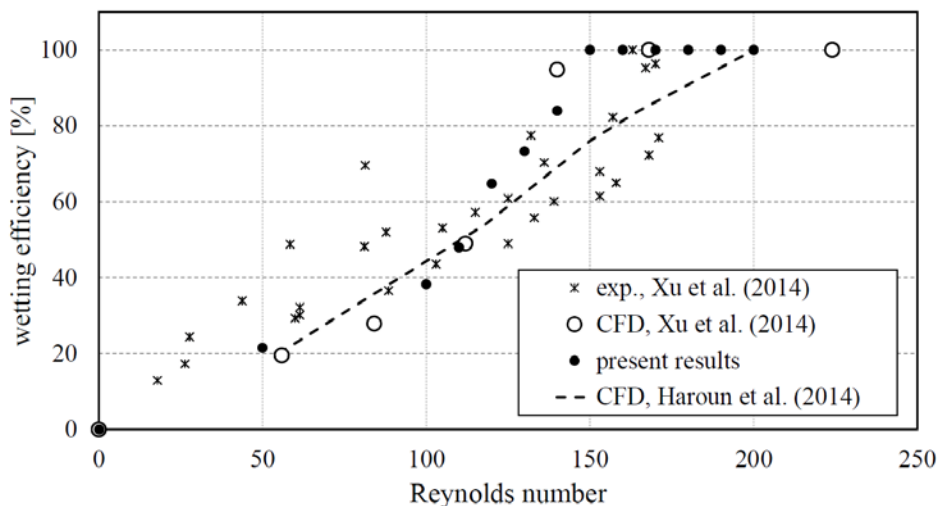

Figure 4. Dependence of the wetting efficiency on the Reynolds number; comparison of the present CFD results with the reference numerical and experimental data of Xu et al. (2014) and Haroun et al. (2014)

The qualitative results of Figure 3 are summarized quantitatively in Figure 4 as a dependence of the wetting efficiency on the Reynolds number. As a reference the already mentioned results of Xu et al. (2014)

(experimental data represented by the asterisks and numerical ones by the empty circles) and Haroun et al. (2014) (CFD data - dashed line) are included in Figure 4. The simulation results obtained in the present work (solid circles) are in a very good agreement with the reference CFD data of Xu et al. (2014). In both cases wetting efficiency increases in a slightly nonlinear way with Re reaching 100% for $Re \approx 150$. Although the experimental results are characterised by noticeable uncertainty (see scatter of points), they in principle indicate linear dependence on Re and deviate from the present results and the CFD data (Xu et al., 2014) which is especially evident in high Re regime. As a consequence critical Reynolds number value, i.e. corresponding to the transition from partially to completely wetted surface, reaches $Re \approx 200$. In contrast good correspondence is found between the experiment of Xu et al. (2014) and the CFD predictions of Haroun et al. (2014). The discrepancies between various CFD data collected in Figure 4 seem to be too large and they require reasonable explanation.

3.2. Impact of the Initial Conditions on the Surface Wettability

The results of the simulations presented in the previous section were obtained for the flow initialized with "wetted" plate, i.e. with the liquid film covering entirely the surface with relevant thickness (see equation 7) and parabolic velocity profile. Similarly Xu et al. (2014) applied "wet plate" initial condition. Although the final solution should be independent of its initialization, it was decided to check whether it may influence the surface wettability. So a series of simulations were conducted for the "dry" plate, i.e. with air filling completely the computational domain.

Temporal evolution of the liquid volume fraction at the plate's surface for both cases and $Re = 50$ is shown in Figure 5 for the selected time instants. Black colour is used here to indicate the liquid phase while white one corresponds to the gas phase. One may easily notice that starting from completely different liquid distributions both flow cases evolve finally to the same morphological structure characterised by a system of short rivulets breaking up into droplets (see Figure 5e). Although the "wetted" plate initialization promotes the formation of a single rivulet (see Figure 5b, bottom), the surface tension forces are strong enough (when compared to inertia) to reduce the rivulet (see Figure 5c, bottom) and to produce a system of droplets originating from different transverse locations of the inlet edge (see Figure 5d, bottom). As a result the wetted portion of the plate is progressively reduced.

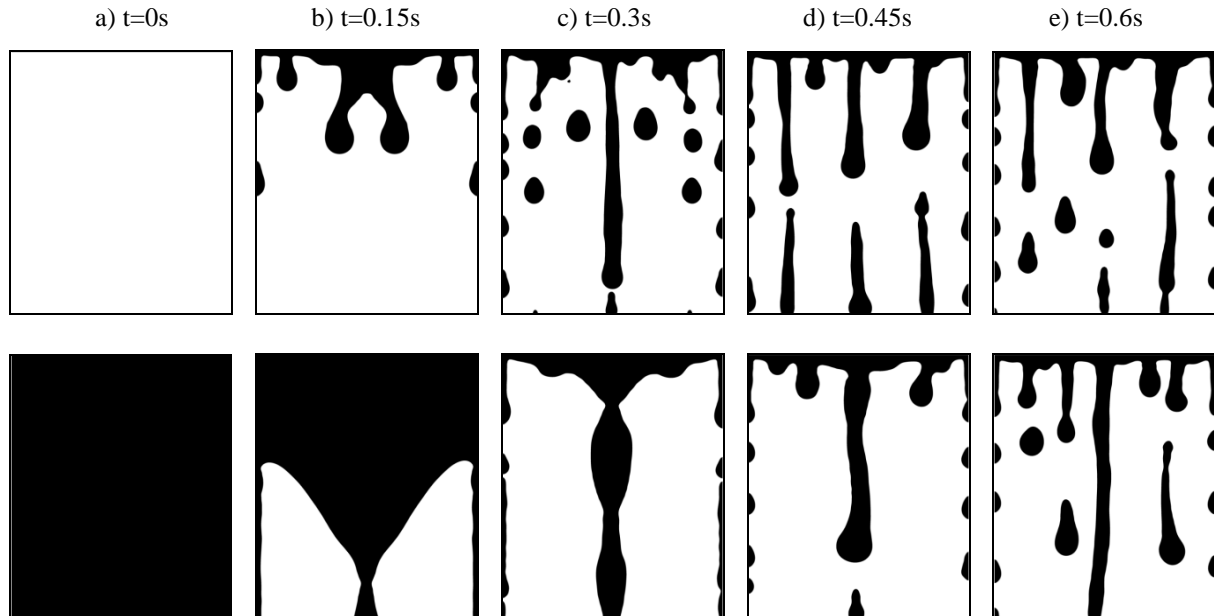| a) t=0s | b) t=0.15s | c) t=0.3s | d) t=0.45s | e) t=0.6s |

Figure 5. Temporal evolution of liquid flow structure for $Re = 50$ and different solution initializations: the top sequence corresponds to the flow initialized with a "dry" plate, while the bottom one to the flow initialized with a liquid film ("wetted" plate)

Similar consistency between "dry" and "wetted" plate initialization can be observed for Re=100. The corresponding time histories are presented in Figure 6. For both cases a quasi-steady state was established with a rivulet formed in the plate's centre. Thus the final flow structure as well as the surface wettability turned out to be

independent of the initial condition applied. This rule turned out to be true for the limited Reynolds number range only. When it exceeded 100 the portion of wetted surface for "dry" initialisation started to decrease when compared to originally "wet" plate. This behaviour was consequently continued for the other Reynolds number values.

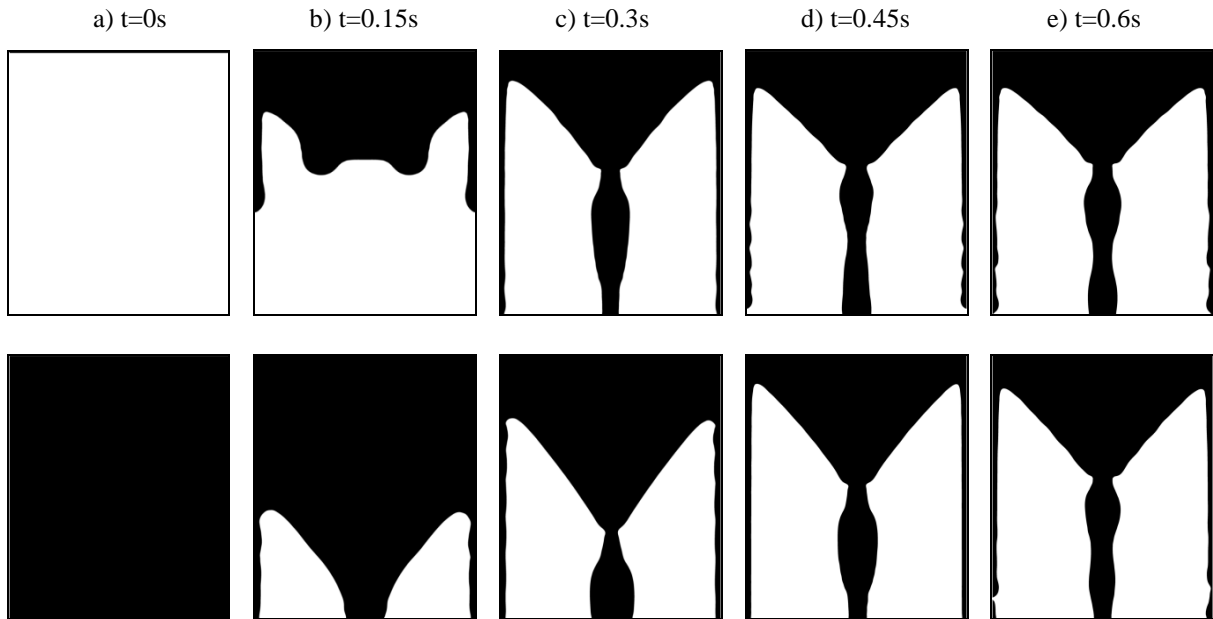| a) t=0s | b) t=0.15s | c) t=0.3s | d) t=0.45s | e) t=0.6s |

Figure 6. Temporal evolution of liquid flow structure for $Re = 100$ and different solution initializations: the top sequence corresponds to the flow initialized with a "dry" plate, while the bottom one to the flow initialized with a liquid film ("wetted" plate)

The effect of initial condition on the wetting efficiency is shown in Figure 7. However, it is presented here as a function of Weber number, i.e. a group number commonly used to analyse the flow phenomena influenced by surface tension. It is defined as:

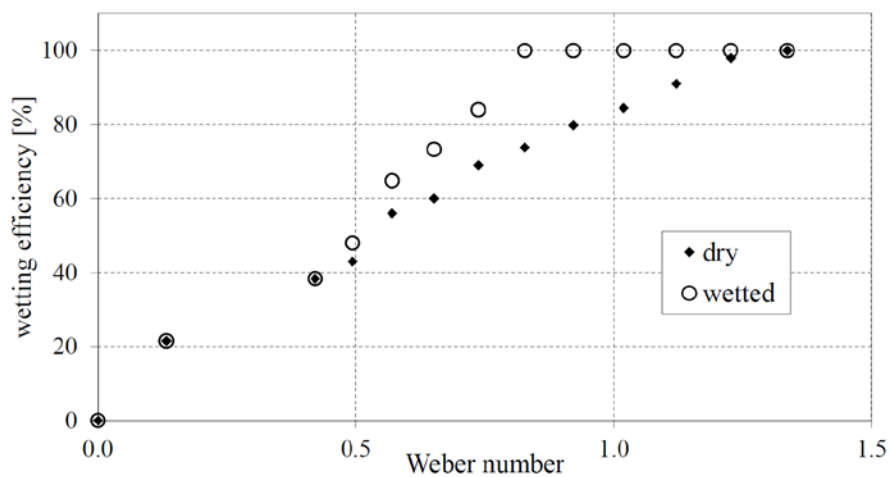$$We = \frac{\rho_L U_{mean}^2 \delta}{\sigma} \qquad (9)$$

Figure 7. Hysteresis of the surface wettability resulting from different initial conditions

As can be seen from Figure 7 the "gap" between 2 differently initialized solutions exists in a quite wide range, i.e. $0.45 < We < 1.3$ and it reaches its maximum extent (equal to 25%) at $We = 0.8$. In order to achieve full wettability for originally dry plate the Weber number had to be increased to 1.3. Such a duality in the evolution

of a flow structure seems to explain the discrepancies identified between various CFD simulations presented in section 3.1 (see Figure 4). Although it is not explicitly stated in their paper Haroun et al. (2014) applied "dry" plate initialization, so their results indicate reduced wettability when compared to the present results and the data of Xu et al. (2014).
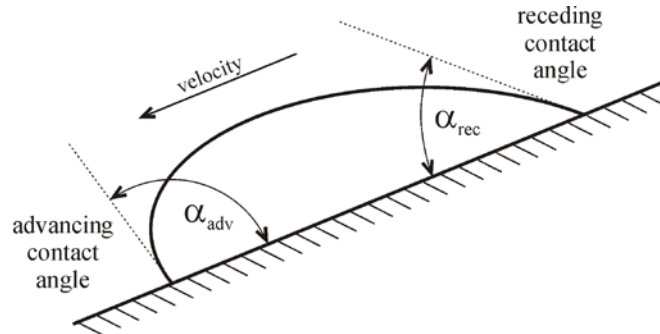

Figure 8. Illustration of the advancing and the receding contact angles for the droplet moving at the inclined flat surface

The hysteresis of the surface wettability could be explained with the variation of the contact angle during the motion of the liquid front. As commonly known the dynamic contact angle of the liquid free surface changes around its static value during the motion of a droplet (Eral et al., 2013). Front of the droplet due to capillary forces is characterised by advancing contact angle while the rear part by the receding one (see Figure 8). The local value of the contact angle depends on many factors and may vary quite significantly. For water the difference between receding and advancing contact angles may even exceed 20 degrees (Eral et al., 2013, Malgarinos et al., 2014).
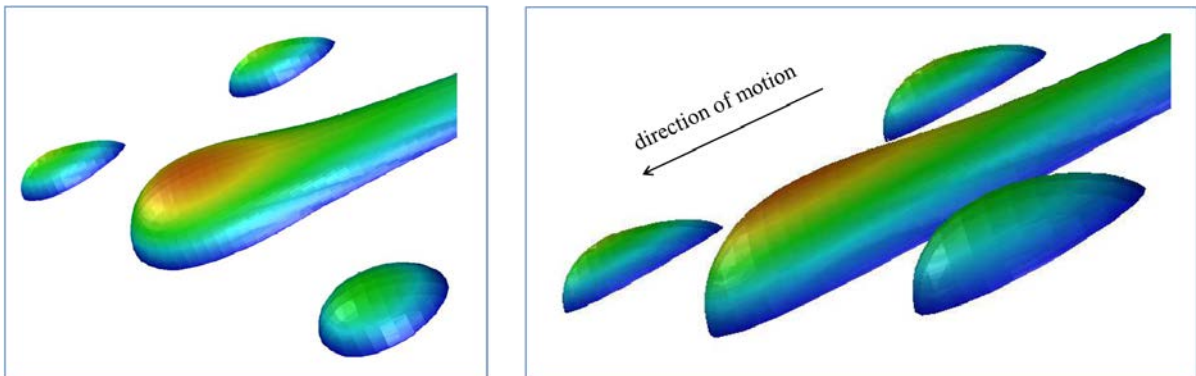

Figure 9. Sample views of the droplet-like flow structure showing the increase of the contact angle in the front of the droplets and rivulet and its decrease at the droplets' rears

Figure 9 presents the sample views of the flow structure for the Reynolds number $Re = 50$ ($We = 0.13$), i.e. for the droplet flow. One can easily notice the observable differences between the contact angles corresponding to the fronts and the rears of the droplets. Magnified views of the free surfaces allowed to estimate the range of the contact angle to $\Delta\alpha = \alpha_{adv} - \alpha_{rec} \approx 15°$. The variation of the contact angle has no consequence on the wetting efficiency for $We < 0.5$ (see Figure 7) with the morphological flow structure dominated by droplets. Regardless the initial conditions (wet or dry plate) the flow has to evolve from the liquid film through the system of rivulets to the cloud of droplets. When the flow structure is finally established and becomes quasi-stationary then the flow "forgets" about its origin and the droplets flow down wetting and dewetting the surface. Reduced wetting at the front of the droplet is compensated by the increased wetting in its rear part. The situation changes for the $We \geq 0.5$ when droplets disappear and the flow becomes stationary with a part of a surface covered with a film (see Figure 3, centre and Figure 3, right). Depending on the flow initialisation the position of the liquid rims are slightly different. For the initially dry surface they are shifted up due to higher contact angle values as the liquid front is moving down during surface wetting. Inversely, for the wetted surface, the liquid front is travelling up,

thus the surface is dewetted with lower contact angles. Such a mechanism explains the hysteresis of the wetting efficiency observed for the rivulet-like flow structure.

4   Summary

Three-dimensional simulations of the liquid flow structure and the surface wettability on a flat inclined plate were carried out for varying Reynolds/Weber number and the initial flow conditions. An Eulerian multiphase one-fluid approach was employed to develop a CFD model in Ansys Fluent environment. Gas-liquid interface was reconstructed with the use of a Volume of Fluid technique. The results were found to be in a good qualitative and quantitative agreement with the available experimental and numerical reference data. It was also shown that the change of the initial condition from the "dry" to the "wetted" plate leads to the increased wettability in the higher Reynolds/Weber number range, in particular for the flow structure dominated by the rivulets. It results in noticeable change of a critical Re/We value determining the upper limit of partial surface wetting. The variation of the dynamic contact angle of the liquid front between the receding and the advancing levels has been found to be responsible for such a wetting efficiency hysteresis.
Full consistency of the results with the reference numerical and experimental data proved the model relevance and its appropriateness for studies of surface wettability. The model is planned to be used in future work to analyse the flow structure and the wetting efficiency for complex geometries of the commercially available structured packings.

Acknowledgements

References

Ansys Inc.: ANSYS Fluent User's Guide. Release 17.0, (2016).

Asendrych D.: Numerical study of surface wettability - the influence of surface tension and contact angle, Proc. 8th International Conference from "Scientific Computing to Computational Engineering", 8th IC-SCCE, Athens, 4-7 July, (2018), 319-326

Asendrych, D.; Niegodajew, P.: Numerical study of the CO_2 absorber performance subjected to the varying amine solvent and flue gas loads. *Chemical Engineering Communications*, 204, 5, (2017), 580-590.

Brackbill, J.U.; Kothe, D.B.; Zemach, C.: A continuum method for modelling surface tension, *Journal of Computational Physics*, 100, (1992), 335-354.

Eral, H.B.; 't Mannetje, D.J.C.M.; Oh, J.M.: Contact angle hysteresis: a review of fundamentals and applications. *Colloid and Polymer Science*, 291, (2013), 247-260.

Haroun, Y.; Legendre, D.; Raynal, L.: Volume of fluid method for interfacial reactive mass transfer: Application to stable liquid film. *Chemical Engineering Science*, 65, (2010), 2896-2909.

Haroun, Y.; Legendre, D.; Raynal, L.: Mass transfer and liquid hold-up determination in structured packing by CFD. *Chemical Engineering Science*, 75, (2012), 342-348.

Haroun, Y.; Raynal, L.; Alix, P.: Prediction of effective area and liquid hold-up in structured packings by CFD. *Chemical Engineering Research and Design*, 92, (2014), 2247-2254.

Hoffmann, A.; Ausner, I.; Repke, J.-U.; Wozny, G.: Detailed investigation of multiphase (gas-liquid and gas-liquid-liquid) flow behaviour on inclined plates. *Chemical Engineering Research and Design*, 84, A2, (2006), 147-154.

Iso, Y.; Huanga, J.; Katoa, M.; Matsunoa, S.; Takano, K.: Numerical and experimental study on liquid film flows on packing elements in absorbers for post-combustion CO_2 capture. *Energy Procedia*, 37, (2013), 860-868.

Lappalainen, K.; Alopaeus, V.; Manninen, M.; Aittamaa, J.: Improved hydrodynamic model for wetting efficiency, pressure drop and liquid holdup in trickle-bed reactors. *Industrial & Engineering Chemistry Research*, 47, (2008), 8436-8444.

Malgarinos, I.; Nikolopoulos, N.; Marengo, M.; Antonini, C.; Gavaises, M.: VOF simulations of the contact angle dynamics during the drop spreading: Standard models and a new wetting force model. *Advances in Colloid and Interface Science*, 212, (2014), 1–20.

Niegodajew, P.; Asendrych, D.: Amine based CO_2 capture - CFD simulation of absorber performance. *Applied Mathematical Modelling*, vol. 40, issues 23-24, (2016), 10222-10237.

Nusselt, W.: Die Oberflächen-kondensation des Wasserdampfes, *Zeitscrift des Vereines Deutschem Ingenieure*, 60, (1916), 541-546.

Sebastia-Saez, J.D.: CFD modelling of post-combustion carbon capture with amine solutions in structured packing columns, *PhD thesis*, Cranfield University, (2016).

Sebastia-Saez, D.; Gu, S.; Ranganathan, P.; Papadikis, K.: 3D modeling of hydrodynamics and physical mass transfer characteristics of liquid film flows in structured packing elements. *International Journal of Greenhouse Gas Control*, 19, (2013), 492-502.

Sebastia-Saez, D.; Gu, S.; Ranganathan, P.: Volume of fluid modeling of the reactive mass transfer of CO_2 into aqueous amine solutions in structured packed elements at microscale. *Energy Procedia*, 63, (2014a), 1229-1242.

Sebastia-Saez, D.; Gu, S.; Ranganathan, P.; Papadikis, K.: Micro-scale CFD study about the influence of operative parameters on physical mass transfer within structured packing elements. *International Journal of Greenhouse Gas Control*, 28, (2014b), 180-188.

Sebastia-Saez, D.; Gu, S.; Ranganathan, P.; Papadikis, K.: Meso-scale CFD study of the pressure drop, liquid hold-up, interfacial area and mass transfer in structured packing materials. *International Journal of Greenhouse Gas Control*, 42, (2015a), 388-399.

Sebastia-Saez, D.; Gu, S.; Ranganathan, P.; Papadikis, K.: Micro-scale CFD modelling of reactive mass transfer in falling liquid films within structured packing materials. *International Journal of Greenhouse Gas Control*, 33, (2015b), 40-50.

Singh, K.R.; Galvin, E.J.; Sun, X.; Singh, K.R.; Galvin, E.J.; Sun, X.: Three-dimensional simulation of rivulet and film flows over an inclined plate: Effects of solvent properties and contact angle. *Chemical Engineering Science*, 142, (2016), 244-257.

Stephan, M.; Mayinger, F.: Experimental and analytical study of countercurrent flow limitation in vertical gas/liquid flows. *Chemical Engineering Technology*, 15, (1992), 51-62.

Subramanian, K.; Wozny, G.: Analysis of hydrodynamics of fluid flow on corrugated sheets of packing. *International Journal of Chemical Engineering*, 2012, (2012), 1-13.

Szulczewska, B.; Zbicinski, I.; Górak, A.: Liquid flow on structured packing: CFD simulation and experimental study. *Chemical Engineering Technology*, 26, (2003), 580-584.

Xu, Y.; Paschke, S.; Repke, J.-U.; Yuan, J., Wozny, G.: Portraying the countercurrent flow on packings by three-dimensional computational fluid dynamics simulations. *Chemical Engineering Technology*, 31, 10, (2008), 1445-1452.

Xu, Y.; Paschke, S.; Repke, J.-U.; Yuan, J.; Wozny, G.: Computational approach to characterize the mass transfer between the counter-current gas-liquid flow. *Chemical Engineering Technology*, 32, 8, (2009), 1227-1235.

Xu, Y.; Repke, J.-U.; Yuan, J.; Wozny, G.: CFD study on liquid flow behaviour on inclined flat plate focusing on effect of flow rate. *Engineering Applications of Computational Fluid Mechanics*, 6, 2, (2012), 186-194.

Xu, Y.; Zhao, M.; Paschke, S.; Wozny, G.: Detailed investigations of the countercurrent multiphase (gas-liquid and gas-liquid-liquid) flow behavior by three-dimensional computational fluid dynamics simulations. *Industrial & Engineering Chemistry Research*, 53, (2014), 7797-7809.

Address: Institute of Thermal Machinery, Częstochowa University of Technology, al. Armii Krajowej 21, 42-200, Częstochowa, Poland
email: darek@imc.pcz.czest.pl